Hindawi
Advances in Materials Science and Engineering
Volume 2021, Article ID 1175621, 15 pages
https://doi.org/10.1155/2021/1175621

Research Article

Mechanical and Microscopic Properties of Graphite/Laterite Nanocomposites

Yuhao Gao,[1,2] **Jianzhong Li**,[1,2] **Yuxin Zhang**,[3] **Xu Sun**,[1,2] **and Leiyong Yang**[1,2]

[1]*Key Laboratory of Metallogenic Prediction of Nonferrous Metals and Geological Environment Monitoring (Central South University), Ministry of Education, Changsha 410083, China*
[2]*School of Geosciences and Info-Physics, Central South University, Changsha 410083, China*
[3]*Guangxi Zhuang Autonomous Region Geological Environment Monitoring Station, Baise 533000, China*

Correspondence should be addressed to Jianzhong Li; lijianzhong@csu.edu.cn

Received 15 May 2021; Revised 11 October 2021; Accepted 13 October 2021; Published 16 November 2021

Academic Editor: Gianfranco Carotenuto

The effectiveness and improvement mechanism of graphite nanoparticles (GN) in strength properties and microstructure characteristics of regional laterite were analysed in this study. Dry density was also taken into consideration, and the effects of graphite nanoparticle (GN) content and dry density were mainly addressed. Triaxial tests, consolidation tests, and penetration tests were used to analyse the effectiveness of different dry densities and graphite nanoparticle mass ratios on the properties of laterite; microscopic methods such as scanning electron microscopy (SEM) tests were used to analyse the improvement mechanism. The results show that the increase in dry density can make the laterite more compact. The large specific surface area and nanoeffects of the graphite nanoparticles (GN) induce the attraction between soil particles after mixing, both of which make the laterite's shear strength; compression index and impermeability have been enhanced to varying degrees. The microscopic tests showed that, as the content of graphite nanoparticles (GN) continues to increase, when it exceeds 1.0%, the attraction between soil particles increases and coarse particles are formed, which leads to the increase of the pores of the soil. In addition, the graphite nanoparticles have a certain degree of lubricity, a high amount of graphite nanoparticles enters the laterite soil layer, increasing the distance and gap between the layers, making it easy to separate the coarse particles from the coarse particles, and the strength increase is reduced. However, it is still stronger than that of the plain laterite.

1. Introduction

Laterite is a brownish yellow and brown regional special clay formed by physical and chemical weathering of carbonate rocks (or rocks rich in iron, silicon, and alumina) under humid and warm subtropical climate [1–4], which is widely distributed in Guangxi Zhuang Autonomous Region in southern China [5, 6]. Due to the special engineering properties of laterite, such as high void ratio, high water content, hard top and soft bottom, loss of water shrinkage, and cracking [7–13], it is easy to induce insufficient foundation bearing capacity, ground collapse, slope cracking, uneven settlement, and other project problems [14–17]. In addition to the disturbance of the stratum developed by the laterite, the unique mechanical properties of the laterite seriously threaten the safety of engineering construction and bring a lot of inconvenience to the construction process [18–22]. Consequently, it has important research significance to improve the properties of laterite.

Traditional admixtures such as fly ash [23–25], lime [26, 27], and cement [28, 29] are used to improve the swelling, permeability, and mechanical strength of clay, while there are engineering problems with poor improvement effects such as slow growth of strength, easy cracking, and poor water stability [30–32] in practical application. Besides, the process of improving soil with fly ash is complicated, its early strength and shrinkage are poor [33], and there is a hidden danger of heavy metal pollution [34], which affects the physical and chemical properties of soil and groundwater [35] and hinders plant life activities [36]. Lime

has problems such as dust, slow strength growth, and poor water stability. Since most of the laterite in South China is acidic, which will interact with lime, its long-term performance will be attenuated after lime improvement [37], and the improvement effect of laterite is poor [38].The economic cost of cement is relatively high. Alkaline dust carrying heavy metals generated in industrial production and engineering applications is scattered in the surrounding soil, water, and vegetation, destroying their physical and chemical properties [39, 40], causing soil environmental pollution along the line [41], threatening agricultural development [42].

Compared with ordinary admixtures, nanomaterials have excellent properties such as small size effect, surface effect, and large specific surface area. Many scholars at home and abroad have conducted research on the modification of nanomaterials and obtained a large number of important results. Sludge was used as a stabilizer and nano-Al_2O_3 as an admixture to study the improvement of their mixture on clay soil. It was found that nano-Al_2O_3 can further improve the plasticity index, compressive strength, and bearing capacity of soil based on sludge. And, the optimal doping amount of nano-Al_2O_3 is determined to be 1% [43]. It can be found that nano-MgO can not only improve the unconfined compressive strength of cement soil but also increase its ductility when nano-MgO was added to cement soft soil to improve the microstructure of stabilized soil. However, excessive use of nano-MgO may cause cracks in the structure. For silt that has undergone freeze-thaw cycles, the improvement effect of nanomaterials is also effective, which is specifically reflected in improving the optimal moisture content, liquid limit, and plastic limit of soil and reducing the maximum dry density and plasticity index [44]. Compared with the untreated soil, the unconfined compressive strength of the soil added with 2% nano-SiO_2 decreases less [45]. In addition to the excellent improvement properties of nano-metal oxides and nano-inorganic compounds, the incorporation of nanomaterials can enhance each material in the composite materials. The filling effect of nano-$CaCO_3$ makes the soil denser and more compact. Hydration promotion reduces the inhibition of cement hydration by the marine environment, and its double positive effect on soil and cement can effectively reduce the corrosion rate of cemented soil in marine environment and improve the compressive strength of cement foundation in marine engineering [46]. Similarly, nanomaterials and other materials form composite materials, which can also jointly ameliorate the basic physical indicators and mechanical strength of soils [47–52].

At present, the investigation and application of nanomaterials in geotechnical engineering mainly focus on nano-metal oxides and nano-metal compounds while rarely involve graphite. Graphite has a high thermal and good durability and stability, which is used widely to strengthen concrete [53] and enhance compressive strength and thermal conductivity [54–56]. The addition of graphite improves tensile cracking and expansion potential of bentonite, improving its strength [57]. It can also enhance the unconfined compressive strength and shear strength of the compacted clay [58], as well as yield strength and hardness of alloy [59]. Carbon nanomaterials, such as graphite nanoparticles (GN), have been used to enhance mechanical properties of composites, due to their unique small size effect, surface effect, and other nanomaterial effects [60–62]. For example, graphene nanoplatelets (GNP) were found to be able to increase the Young's modulus, tensile yield strength, and tensile breaking strength and reduce tensile elongation at break of composite materials [63]. Meng et al. [64] observed that the tensile strength, flexural strength, and toughness of composites containing concrete-based graphite nanoparticles (GN) are higher than those of the plain concrete. With the addition of graphite nanoparticles (GN), the antiwear performance and extreme-pressure performance of mineral oil additives were significantly improved [65]. On the other hand, nanographite powder (NGP) has a significant effect on enhancing the tensile strength, compressive strength, and hardness of alloy, which is due to grain refinement and compelling of stack transfer [66].

In recent years, researchers have focused on various forms of graphite, and a few literature studies have reported that adding graphite nanoparticles can significantly improve clay, especially laterite. The changes in the strength, elastoplasticity, and hydraulic conductivity of laterite after the addition of graphite nanoparticles need to be further studied.

Nanoscale graphite powder has strong adsorption, high temperature resistance, structural stability, and other properties. Considering that nanoscale graphite powder can fill the pores of laterite, its strong adsorption can increase the cementation of laterite, while its structure is stable and unchanging, and it can adapt to changes in the external environment.

In summary, this study added the admixture of graphite nanoparticles (GN) to the laterite, took a series of consolidated undrained triaxial tests, standard consolidation tests, variable head penetration tests, and scanning electron microscopy (SEM) tests to further study the influence of dry density and GN on the material composition, mechanical properties, and microstructure of laterite, as well as the microscopic mechanism that causes changes in the mechanical properties of laterite.

2. Materials

2.1. Laterite. The soil samples used in this study are all remodeled samples prepared from disturbed laterite samples. The soil samples were taken from a foundation pit in a construction site in Yanshan District, Guilin City, Guangxi Zhuang Autonomous Region, southern China. The landform is a karst plain, and the soil samples are buried deep 2.0–3.0 m, overlying arable soil, underlying limestone. The soil is reddish brown and yellowish brown, whose basic physical properties are shown in Table 1. The disturbed laterite samples are stored in the dark and air-dried naturally. It is then milled and passed through a No. 10 sieve to form a soil sample to be prepared.

Table 1: Physical properties of laterite.

Description	Value
Relative density	2.71
Liquid limit (%)	53.53
Plastic limit (%)	34.02
Plasticity index (%)	19.51
Maximum dry density (g/cm^3)	1.56
Optimum moisture content (%)	30.23

2.2. Graphite Nanoparticles (GN). The XF011 type flake GN produced by Nanjing XFNANO Materials Tech. Co., Ltd were chosen for the experiments, which have good macro-uniformity. Table 2 shows the basic parameters of XF011 type flake GN.

The company performed transmission electron microscopy and SEM characterization tests on XF011 type GN (Figures 1 and 2). The GNs are in the form of flakes, the particles are evenly distributed, the width is about 5 μm, and the thickness reaches the nanometer level.

3. Experimental Investigations

3.1. Undrained and Consolidation Shear Test. The TSZ-1 strain control triaxial tester produced by Nanjing Soil Instrument Factory was selected for the test. When preparing the GN-laterite samples, the natural air-dried laterite sample that has passed through the No.10 sieves was taken, GN was added. Adopted the mass ratio (the mass ratio of dry GN to laterite dry soil, M) 0%, 0.5%, 1.0%, and 2.0%, respectively, and mixed them evenly. The mixed samples of GN-laterite at various mass ratios were mixed with an appropriate amount of distilled water to reach a state of 30.0% optimal moisture content, and then the soil samples were sealed and kept moisturized for 24 hours to remeasure the moisture content. The GN-laterite mixed samples with a dry density (ρ_d) of 1.30 g/cm^3, 1.40 g/cm^3, and 1.50 g/cm^3 were weighed and compacted in four layers by compaction method. After each layer was compacted to the corresponding height, the surface of each layer was roughened to prepare 48 samples of Ø39.1 × 80 mm GN-laterite column specimens. The samples were pumped for 2 hours by the air extraction saturation method and saturated for 12 hours until the saturation exceeded 95%. Three confining pressures of 100 kPa, 300 kPa, and 500 kPa are selected for triaxial consolidation undrained test. The consolidation process was completed with the pore water pressure dissipating more than 95% as the completion standard. The shear rate of 0.9 mm/min was selected for the shear process, which was terminated until the axial strain reaches 20%.

3.2. Standard Consolidation Test. The standard consolidation test was carried out with WG type consolidation meter produced by Nanjing Soil Instrument Factory. In the preparation of samples, the natural air-dried laterite samples passing No. 10 sieves were selected, and the GN was mixed with four mass ratios of 0%, 0.5%, 1.0%, and 2.0%, and water content was also 30.0%. The sample preparation adopted the compression method. The size of each sample was Ø61.8 × 20 mm. the required wet soil and GN mass were weighed based on the set dry densities of 1.30 g/cm^3, 1.40 g/cm^3, and 1.50 g/cm^3. The soil was poured into the sampler with a ring knife preinstalled, smoothed the surface of the soil sample, pressed the soil into the ring knife with static pressure to take out the sample, and prepared a total of 16 samples. Finally, the prepared consolidated samples were pumped for 2 hours by the air-saturation method, saturated for 12 hours until the saturation exceeded 95%. After the installation of the samples was completed, start loading. The pressure shall be loaded in nine levels of 12.5 kPa, 25 kPa, 50 kPa, 100 kPa, 200 kPa, 400 kPa, 800 kPa, 1600 kPa, and 3200 kPa. When the consolidation exceeded 24 hours under each grade of pressure and the deformation of the sample was no more than 0.01 mm per hour, the next level of pressure was applied.

Table 2: Properties of GN.

Description	Value
Purity	99.9
Shape	Flake powder
Thickness, nm	<40
Diameter distribution, μm	3–6

3.3. Variable Head Permeability Test. TST-55 permeameter produced by Nanjing Soil Instrument Factory was used in the experiment. The water head of the permeability test with variable water head was set as 2.0 m. During the preparation of the GN-laterite used in the test, the natural air-dried laterite passed through No.10 sieves was mixed well with the GN whose mass ratios were 0%, 0.5%, 1.0%, and 2.0% respectively. The water content was set as 30.0%, and the dry density was selected as 1.40 g/cm^3. The size of each sample was calculated, the required mass of wet GN-laterite was weighed, poured them into the sample holder with a ring knife installed in advance, smoothed the sample surface, and compacted the sample into 8 samples with the size of Ø61.8 × 40 mm in three layers. Finally, the prepared consolidation samples were pumped for saturation, then pumped for 2 hours, and saturated for 12 hours until the saturation exceeded 95%. The samples were loaded into the permeameter and kept exhausting. After the drain valve at the top of the permeameter overflowed for 2 hours, the initial water head, time, and water temperature was recorded every 48 hours. After three consecutive recordings, the water head was raised to 2.0 m, and the test was stopped after five times of raising the water head.

3.4. Scanning Electron Microscope (SEM) Test. The micromorphology of laterite and GN-laterite was observed by SEM test. The structural characteristics of the samples were obtained by using Sigma 300 SEM produced by Zeiss company, and the voltage was set at 3 kV. After triaxial tests, the soil samples with a dry density of 1.40 g/cm^3, mass ratio of 0% laterite, and 1.0% GN-laterite were naturally dried, cut into 20 × 10 × 10 mm rectangular soil samples, and then broken into 10 × 10 × 10 mm cube. The cross section was

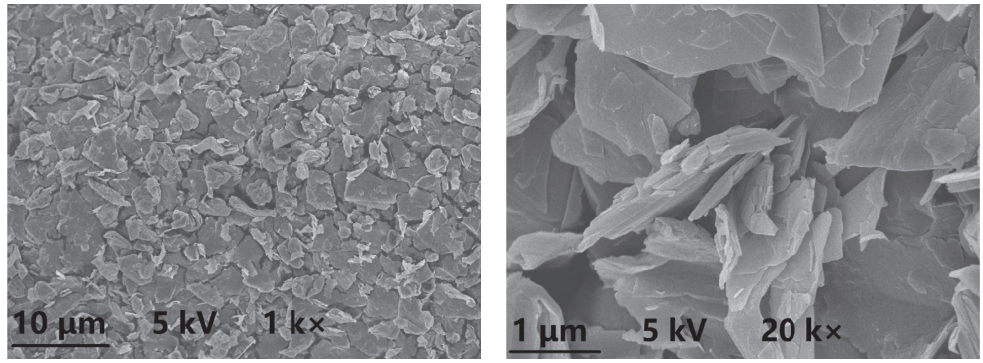

(a) (b)

Figure 1: SEM of GN.

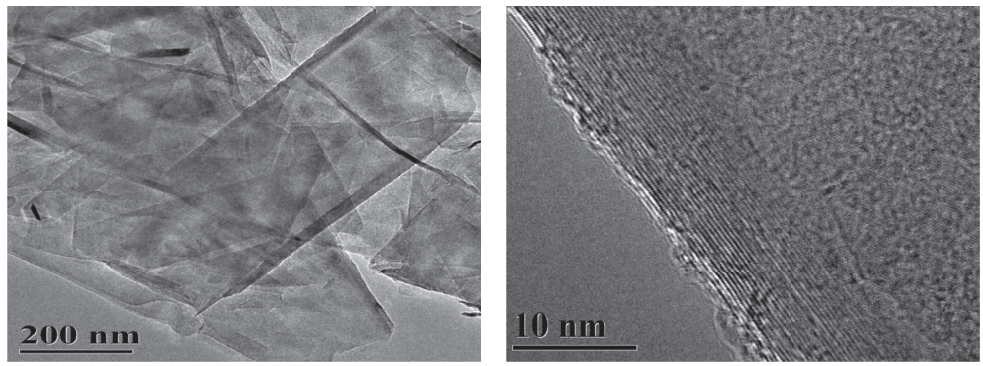

(a) (b)

Figure 2: TEM of GN.

used as the scanning surface, and the magnification was 1 000 times and 4 000 times.

4. Results and Discussion

4.1. Strength Characteristic Analysis. The shear failure forms of GN-laterite with different mass ratios are all bulging failures (Figure 3).

When the GN content is at the same level, the relationship between principal stress difference and axial strain of triaxial consolidated undrained test are shown in Figures 4(a)–4(c) and Figures 4(e)–4(g). The figures show that the dry density has a certain influence on the stress-strain curve of GN-laterite, which is mainly manifested in that the principal stress difference increases with the axial strain, and the relationship curve ($M = 1.0\%$) presents different forms due to the influence of dry density. Under the same dry density, with the increase of confining pressure, the slope of the relationship between the principal stress difference and axial strain of GN-laterite shows an upward trend. Under the same confining pressure, with the increase of dry density, the main stress difference of GN-laterite and the slope of axial strain relationship curve have a certain upward trend, and the rising range is similar. The curves of the relationship between principal stress difference and axial strain of GN-laterite with three different dry densities show approximate strain hardening characteristics, and the morphology exhibits an approximate hyperbola. The peak point also appears before the strain is 5%, and the slope of the curve changes slowly after the peak point.

When the dry density is at the same level, the relationship between principal stress difference and axial strain of triaxial consolidated undrained test shows that the GN content has a certain influence on the stress-strain curve of laterite, which mainly shows that the relationship curve (dry density is $1.40\,g/cm^3$) presents different forms with the increase of axial strain (Figures 4(b), 4(d), 4(f), and 4(h)). When the GN mass ratio is 0%, the relationship curve between principal stress difference and axial strain presents ideal plastic characteristics when the confining pressure is below 300 kPa. There is an obvious peak point, and the slope of the curve after the peak point is close to horizontal. When the confining pressure is 500 kPa, the relationship curve between principal stress difference and axial strain presents strain hardening characteristics, and its shape is approximately hyperbolic with less obvious peak point. When the GN mass ratio is 0.5%, the relationship characteristic between principal stress difference and axial strain is below 300 kPa is like that of the curve when the GN mass ratio is 0%, and the slope of the curve decreases from large to horizontal after the peak point. When the confining pressure is 500 kPa, the principal stress difference and the axial strain

(a) (b) (c) (d)

Figure 3: GN-laterite samples after triaxial test, (a) $M = 0\%$, (b) $M = 0.5\%$, (c) $M = 1.0\%$, (d) $M = 2.0\%$.

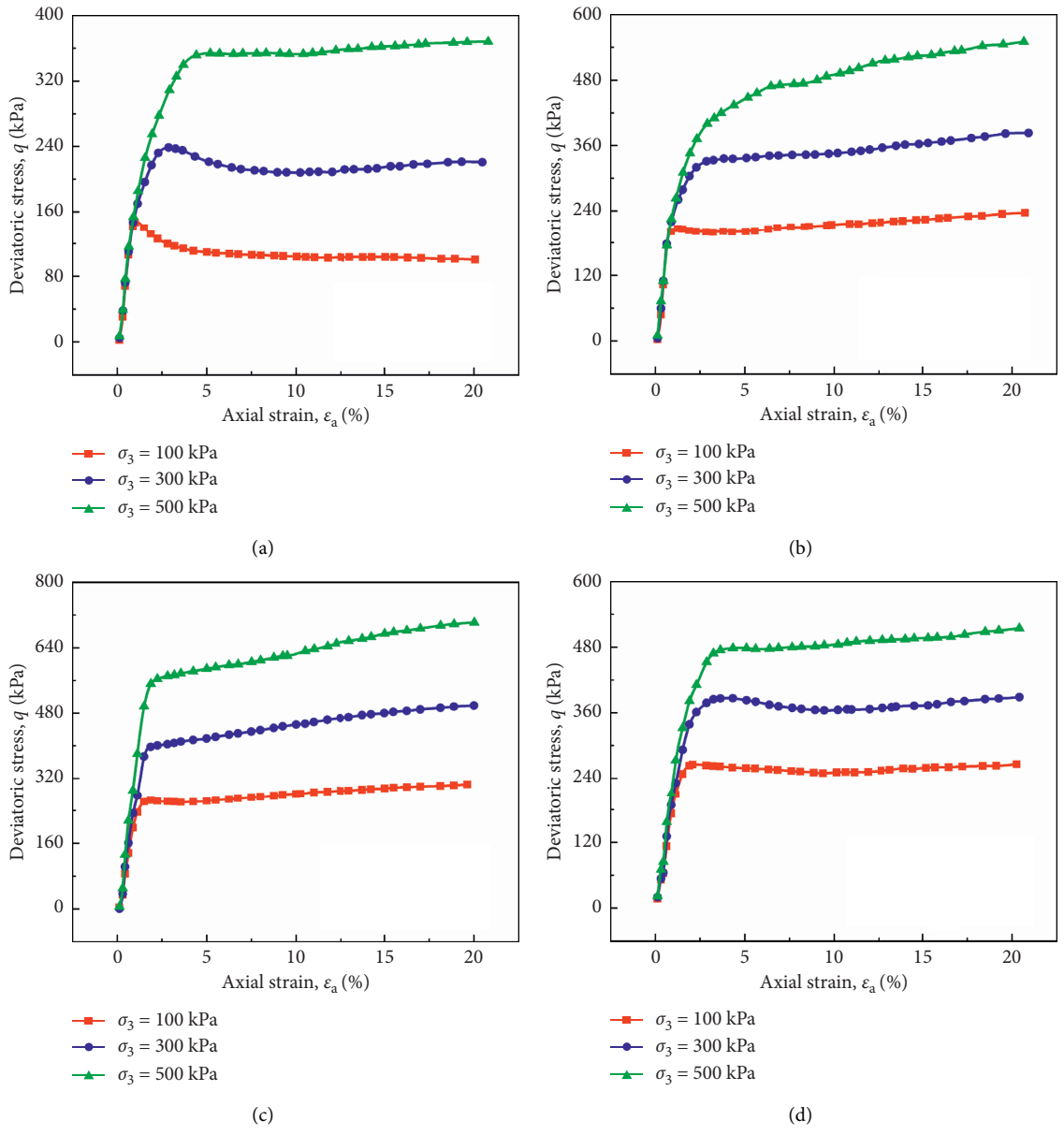

Figure 4: Continued.

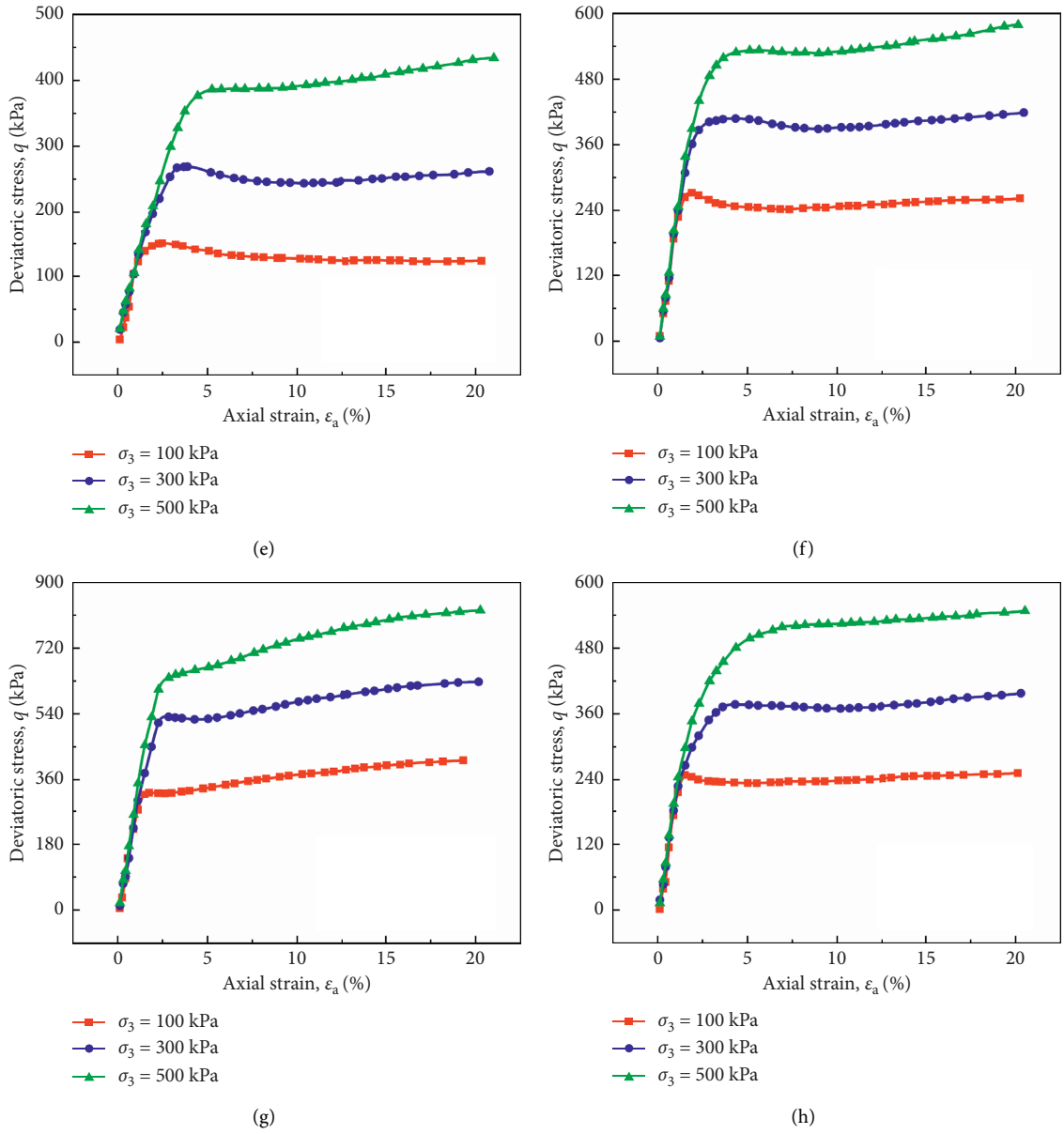

Figure 4: Stress-strain curves of laterite and GN-laterite, (a) $\rho_d = 1.30\ g/cm^3$, $M = 0\%$, (b) $\rho_d = 1.40\ g/cm^3$, $M = 0\%$, (c) $\rho_d = 1.50\ g/cm^3$, $M = 0\%$, (d) $\rho_d = 1.40\ g/cm^3$, $M = 0.5\%$, (e) $\rho_d = 1.30\ g/cm^3$, $M = 1.0\%$, (f) $\rho_d = 1.40\ g/cm^3$, $M = 1.0\%$, (g) $\rho_d = 1.50\ g/cm^3$, $M = 1.0\%$, and (h) $\rho_d = 1.40\ g/cm^3$, $M = 2.0\%$.

relationship curves show strain-hardening characteristics, which is approximately hyperbolic. The slope of the curve fluctuates slightly. When GN are added and the mass ratio was 1.0% and 2.0%, the relationship between principal stress difference and axial strain curve shows approximately ideal plastic characteristics at each confining pressure, and its shape shows an approximate hyperbolic line with obvious peak point. The slope of the curve still changes after the peak point while eventually tends to horizontal.

The shear strength of soil consists of frictional strength and cohesive strength according to Mohr–Coulomb strength theory. The peak principal stress difference is taken as the stress state at the failure point. If there is no obvious peak, the corresponding principal stress difference at the slope drop point on the curve or when the axial strain is 15% is taken as the failure point in this study. Based on the difference of the principal stress at the failure point measured by the test, the shear stress is taken as the ordinate and the normal stress as the abscissa. The stress circle is drawn on the plane of shear stress and normal stress, and the strength envelope of the stress circle under different surrounding pressures is drawn according to the linear Mohr–Coulomb theory to obtain the consolidated undrained strength parameters of GN-laterite (Figure 5).

From Figure 5, we can intuitively obtain the complete two-dimensional stress state of the failure surfaces of GN-laterite samples when they were damaged, that is, in the limit equilibrium state. Through the slope and intercept of the common tangent (shear strength envelope) of Mohr circle

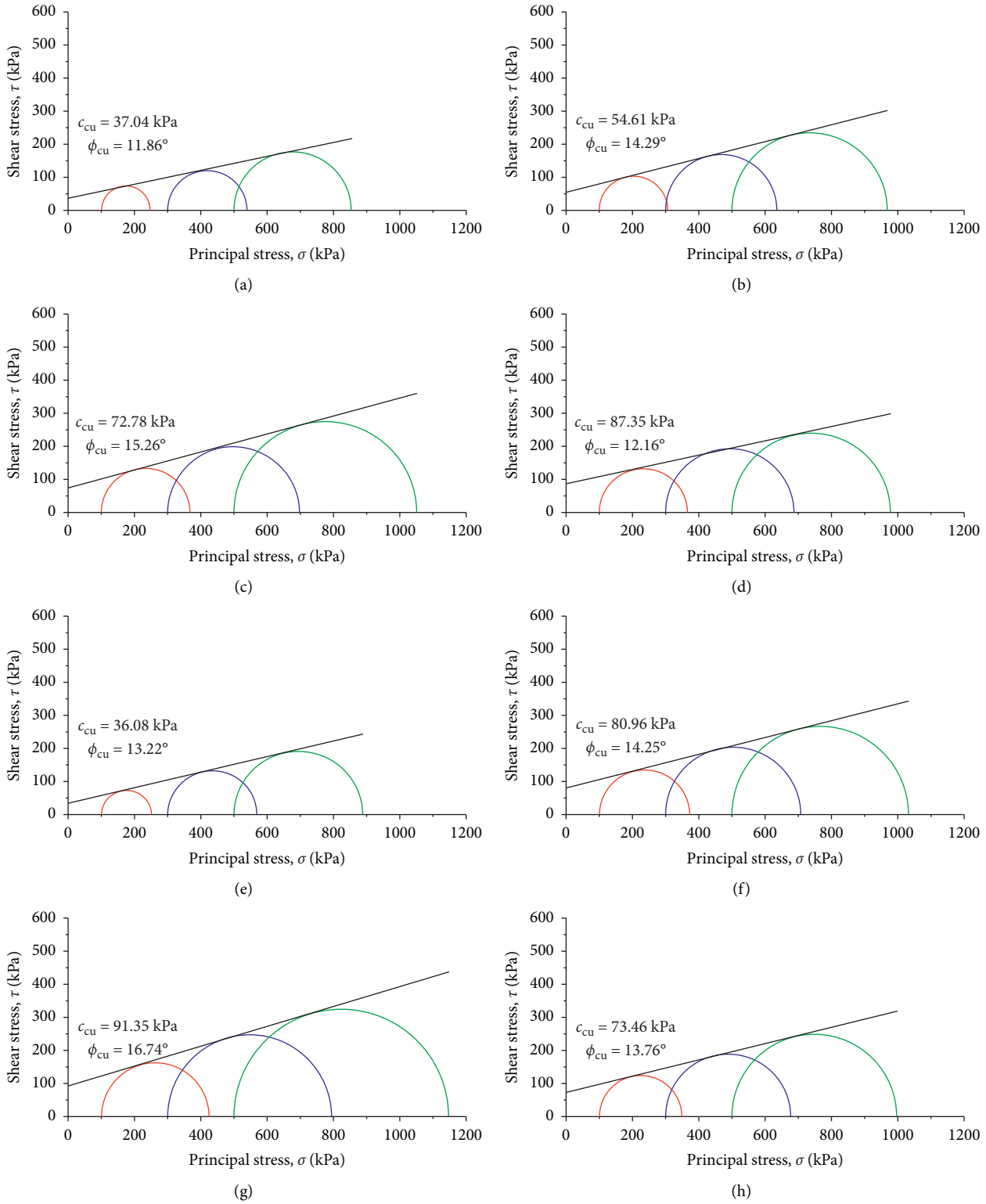

FIGURE 5: Mohr–Coulomb failure envelope of laterite and GN-laterite (red lines mean $\sigma 3 = 100$ kPa, blue lines mean $\sigma 3 = 300$ kPa, green lines mean $\sigma_3 = 500$ kPa, and black lines mean the damage envelope.), (a) $\rho_d = 1.30$ g/cm^3, $M = 0\%$, (b) $\rho_d = 1.40$ g/cm^3, $M = 0\%$, (c) $\rho_d = 1.50$ g/cm^3, $M = 0\%$, (d) $\rho_d = 1.40$ g/cm^3, $M = 0.5\%$, (e) $\rho_d = 1.30$ g/cm^3, $M = 1.0\%$, (f) $\rho_d = 1.40$ g/cm^3, $M = 1.0\%$, (g) $\rho_d = 1.50$ g/cm^3, $M = 1.0\%$, and (h) $\rho_d = 1.40$ g/cm^3, $M = 2.0\%$.

under different confining pressures, the cohesion and internal friction angle of GN-laterite sample can be obtained. In this way, the relationship between the shear strength (including cohesive strength and friction strength) of the sample and the confining pressure, GN content, and dry density can be obtained, as shown in Figures 6 and 7.

The figures show that the shear strength increases linearly with the increase of confining pressure and dry density. With the change of the GN mass ratio, the shear strength first increased and then decreased, and there is peak shear strength. The GN mass ratio corresponding to the peak principal stress difference is defined as the optimal mass ratio, which means that the maximum shear strength value can be obtained by the triaxial consolidation undrained test method under this mass ratio. When the GN mass ratio is between 1.0% and 2.0%, and close to 1.0%, the shear strength reaches the maximum. When the GN content is relatively low, the shear strength increases with the increase of the mass ratio, and then the slope of the curve begins to gradually decrease. When the GN mass ratio continues to increase until it reaches the upper limit of the optimal mass ratio of 2.0%, the shear strength of GN-laterite will be significantly reduced.

The cohesion parameters of GN-laterite shows that the cohesion strength increases with the increase of dry density (Figure 8). The influence of dry density on plain laterite is approximately linearly increasing. The GN-laterite soil showed a gradual decrease in the rate of increase, and the rate attenuation appeared after the dry density was greater than 1.40 g/cm^3, that is, when the dry density was greater than 1.40 g/cm^3, the enhancement effect of the dry density on the GN-laterite was attenuated. Figure 9 shows that the content of GN has a significant influence on the cohesive force of laterite. The cohesion increases with the increase of the content and then reaches the peak near 0.5% during the content of GN is between 0% and 0.5%. While the mass ratio is 1.0%, the cohesion decreases but is close to the peak, and the shear strength reaches the peak when the mass ratio is 1.0%. When the content of GN continues to increase to 2.0%, the cohesion decreases obviously, but it is higher than that of the laterite without GN, which indicates that the appropriate amount of GN can significantly improve the cohesion of laterite. The influence of GN on the cohesion of laterite is that the nanoproperties and adsorption properties of GN play a major role.

Figure 10 shows that, as the dry density increases, the friction strength increases linearly, but the slope will change differently. With the increase of dry density, the increasing slope of laterite internal friction angle decreases, while the increasing amplitude of GN- laterite internal friction angle increases. As shown in Figure 11, the GN has a certain influence on the friction strength parameters, but the influence degree is small. The value of the internal friction angle changes within the range of 2° with the change of the GN mass ratio. It can be inferred that when the dry density is at the same level, the effect of GN on the friction strength of laterite is relatively small, whether it is caused by the mutual movement and occlusion of particles or by the attraction of physical and chemical action on the surface of particles.

4.2. Deformation Characteristics Analysis. The variation of compression modulus and compression coefficients with different dry densities and GN mass ratios calculated by standard consolidation tests is shown in Figures 12–15. As

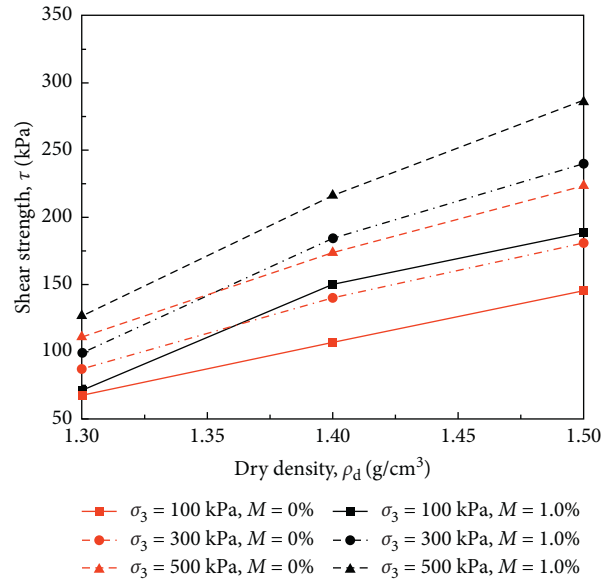

Figure 6: Effect of dry density on shear strength.

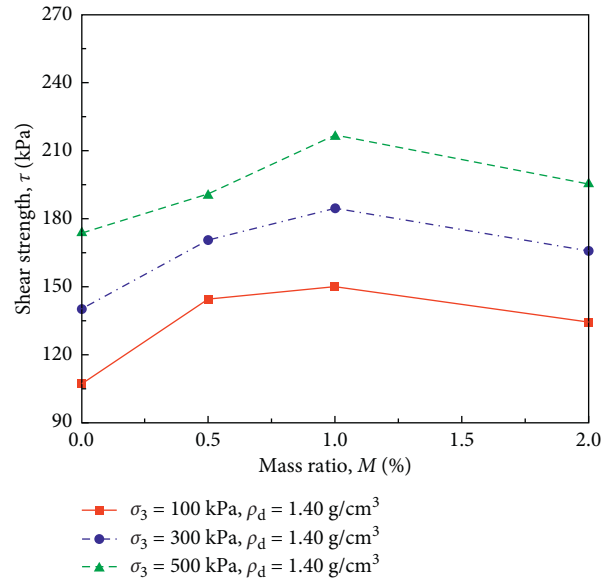

Figure 7: Effect of mass ratio on shear strength.

shown in Figures 12 and 13, the GN-laterite samples with different GN mass ratios (M = 0%, M = 0.5%, M = 1.0%, and M = 2.0%) are all low compressibility soils. The compressive modulus of GN-laterite and plain laterite both increase with the change of dry density. The difference is that the increasing slope of the compressive modulus of plain laterite increases with the increase of dry density, while the increase of GN-laterite is linear. When the mass ratio of GN is 0.5% and 1.0%, the increasing slope of the compressive modulus on GN-laterite is the same, while when the mass ratio is 2.0%, the compressive modulus of laterite increases greatly, which shows that the mixing GN can reduce the compressibility of laterite.

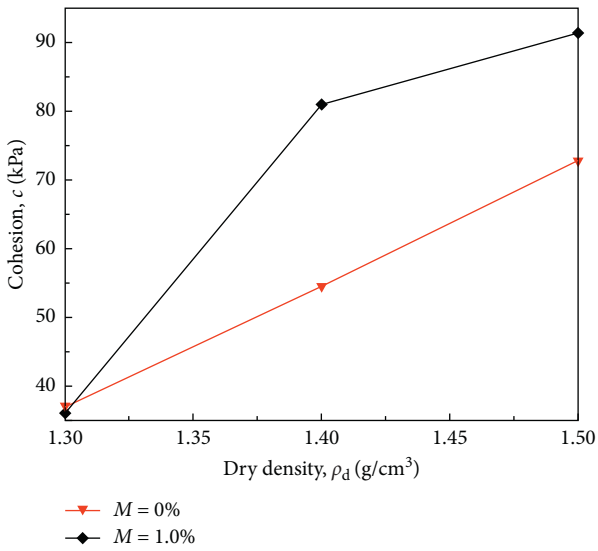

Figure 8: Effect of dry density on cohesion.

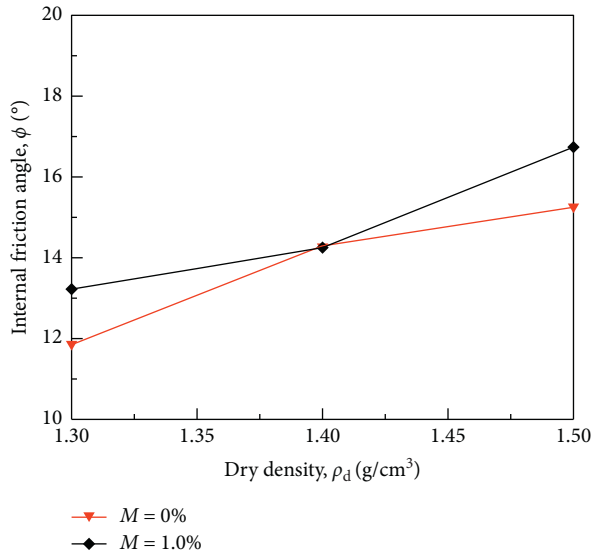

Figure 10: Effect of dry density on internal friction angle.

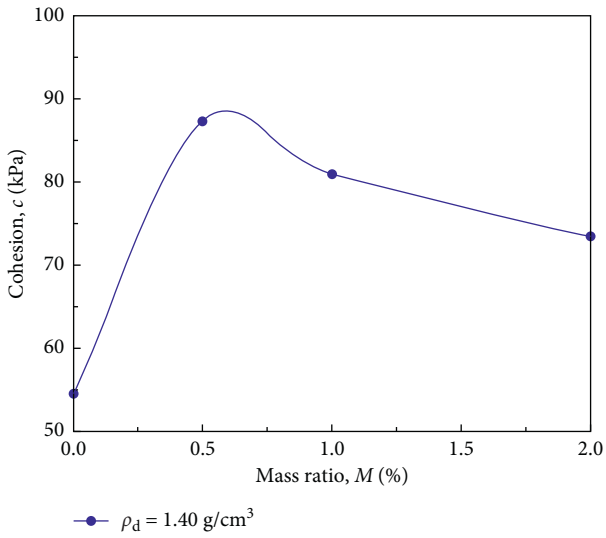

Figure 9: Effect of mass ratio on cohesion.

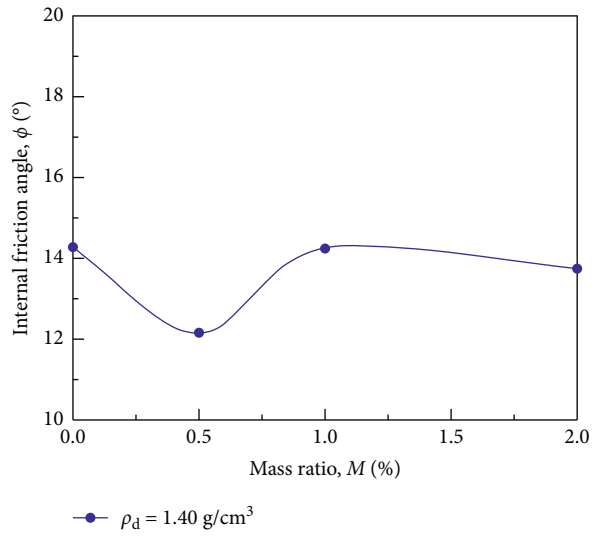

Figure 11: Effect of mass ratio on internal friction angle.

It can be seen intuitively from Figure 14 that the compression coefficients of GN-laterite ($M = 1.0\%$) and plain laterite with different dry densities decrease with the increase of dry density, and the reduction range is decreasing.

When the dry density is 1.30 g/cm^3, the compressibility coefficient of GN-laterite ($M = 1.0\%$) is reduced by 0.013 MPa^{-1} compared with plain laterite. While the dry density is 1.40 g/cm^3, the compressibility coefficient of GN-laterite ($M = 1.0\%$) is reduced by 0.008 MPa^{-1} compared with plain laterite. The compressibility coefficient of GN-laterite ($M = 1.0\%$) is reduced by 0.001 Mpa^{-1} compared with plain laterite when the dry density is 1.50 g/cm^3. Figure 15 shows that, as the GN mass ratio increases successively, the compressibility of GN-laterite decreases in turn. When the GN mass ratio is 0.5%, the compression coefficient of GN-laterite decreases slightly, while at 1.0% and 2.0%, the compression coefficient of GN-laterite decreases greatly. The larger the GN mass ratio, the better the compression performance on GN-laterite. On the one hand, it shows that GN can reduce the compressibility coefficient of laterite; on the other hand, with the increase of dry density, the compressibility coefficient of GN-laterite is closer to that of plain laterite when the dosage ratio is 1.0%, that is, with the increase of dry density, the effect of GN on reducing the compressibility coefficient of laterite gradually weakens.

4.3. Permeability Analysis. The evaluated permeability coefficients of different GN mass ratios are shown in Figure 16. When the dry density of the soil sample is 1.40 g/cm^3, the permeability coefficient of GN-laterite decreases with the increase of the GN mass ratio. The addition of GN has a

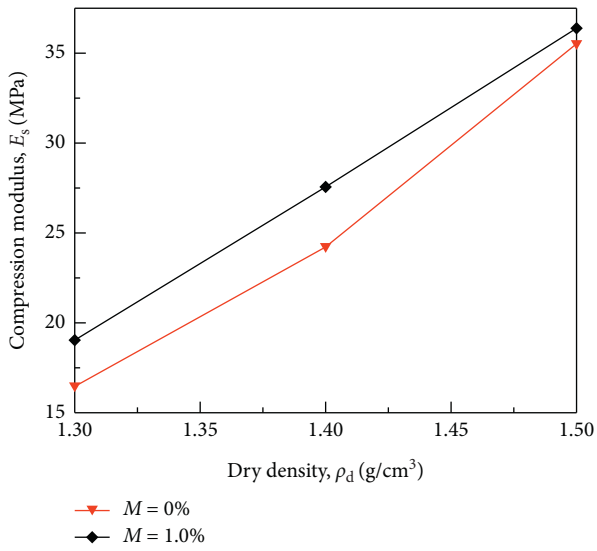

Figure 12: Effect of dry density on compression modulus.

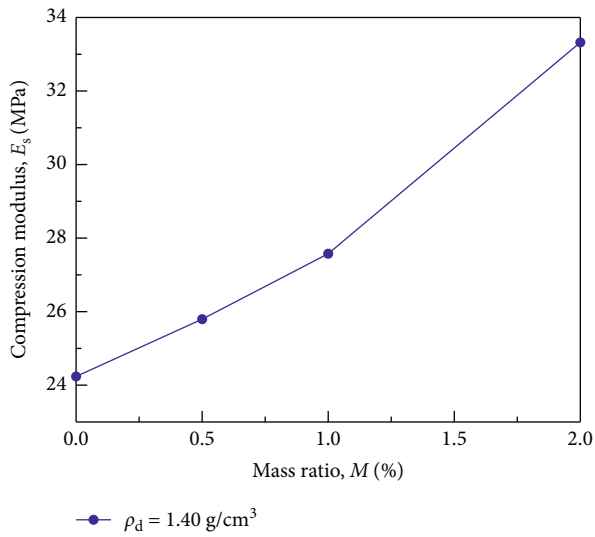

Figure 13: Effect of mass ratio on compression modulus.

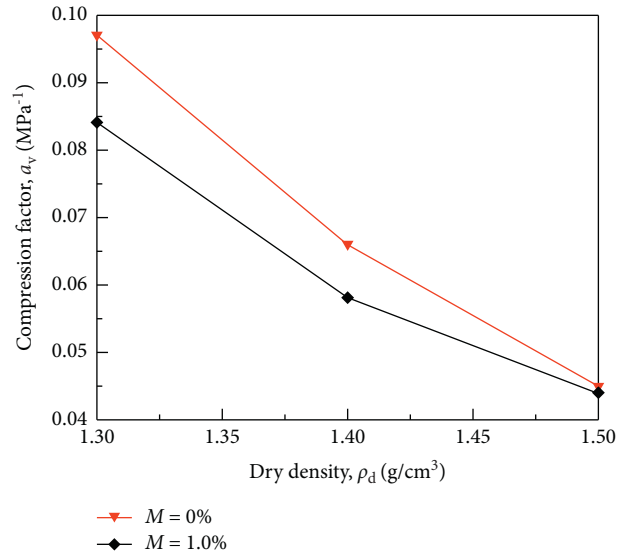

Figure 14: Effect of dry density on compression factor.

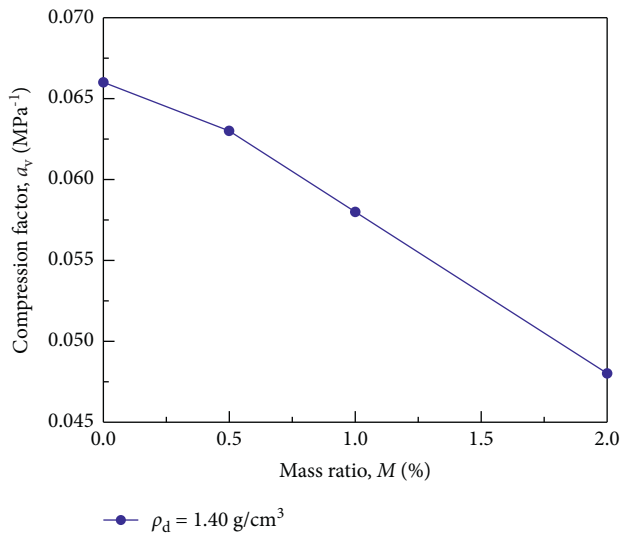

Figure 15: Effect of mass ratio on compression factor.

significant effect on the permeability coefficient of the laterite. A small amount of GN ($M = 0.5\%$) can improve the permeability coefficient of laterite better compared with the plain laterite. Compared with plain laterite, the permeability coefficients of the mass ratios of 0.5%, 1.0%, and 2.0% GN-laterite are reduced by 0.73×10^{-6} cm/s, 1.94×10^{-6} cm/s, and 2.47×10^{-6} cm/s; the decreasing rate first increases and then decreases, which indicates that the greater the GN mass ratio is, the greater the change range of GN-laterite permeability coefficient is, but the changing rate is the best when the GN mass ratio is 1.0%, and the decreasing range decreases with the increase of GN mass ratio.

4.4. Microscopic Morphology Analysis. The microstructure of laterite and GN-laterite was obtained by SEM, as shown in Figure 17. The soil particles of Guilin laterite are angular and rough in surface. The clusters and clusters are connected to each other to form a structural framework. The contact surface between the clusters is small, the connection between the clusters is weak, and the internal structure is relatively loose. The large pores and cracks between the granules are extremely developed, forming an overhead structure. After magnification of 4 000 times, it is observed that the basic structural units in the laterite pellets are flakes and loose grains. The flake structural units have clear outlines, different sizes, and are stacked. There are many small pores in the pellets, which are honeycomb or spongy.

It can be seen from the SEM (Figure 17) that, as the dry density increases, the compactness of the laterite increases, and small particles fill small pores that also helps the fine GN to fill the pores of the soil, which brings about the improvement of shear strength and compression performance.

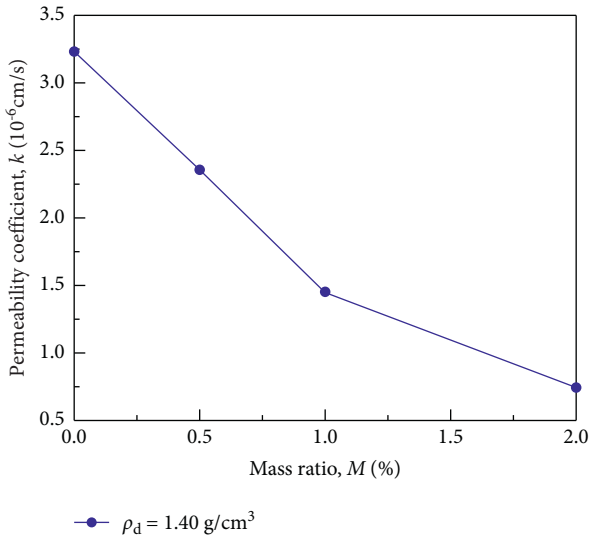

Figure 16: Effect of mass ratio on permeability coefficient.

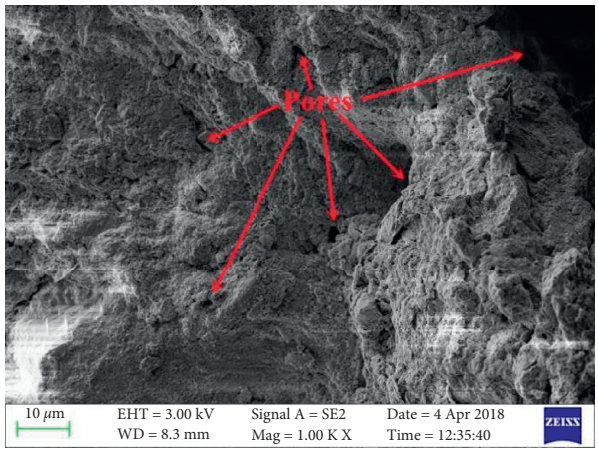

(a)

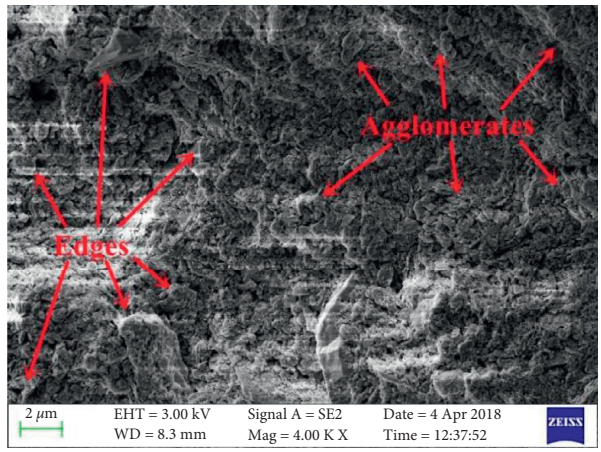

(b)

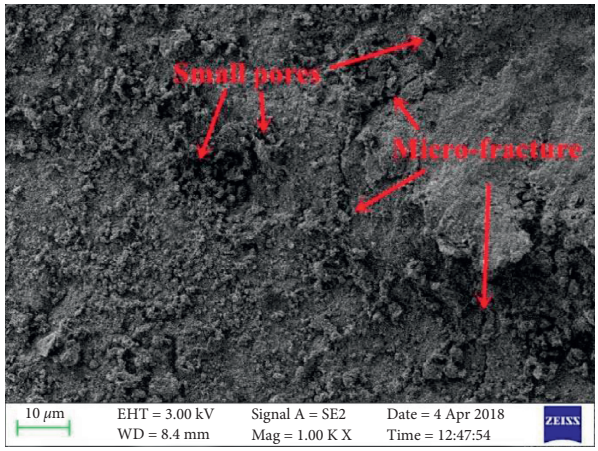

(c)

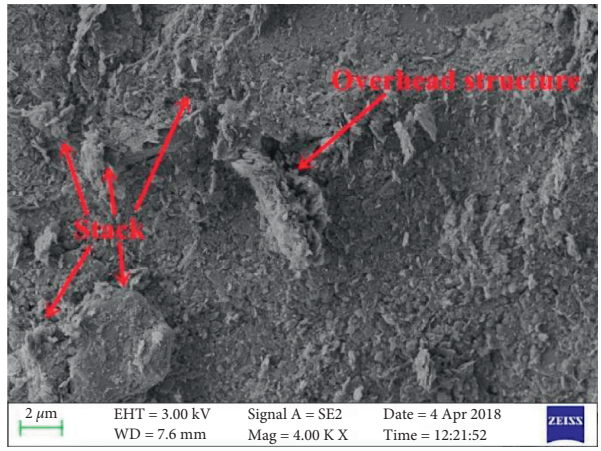

(d)

Figure 17: Continued.

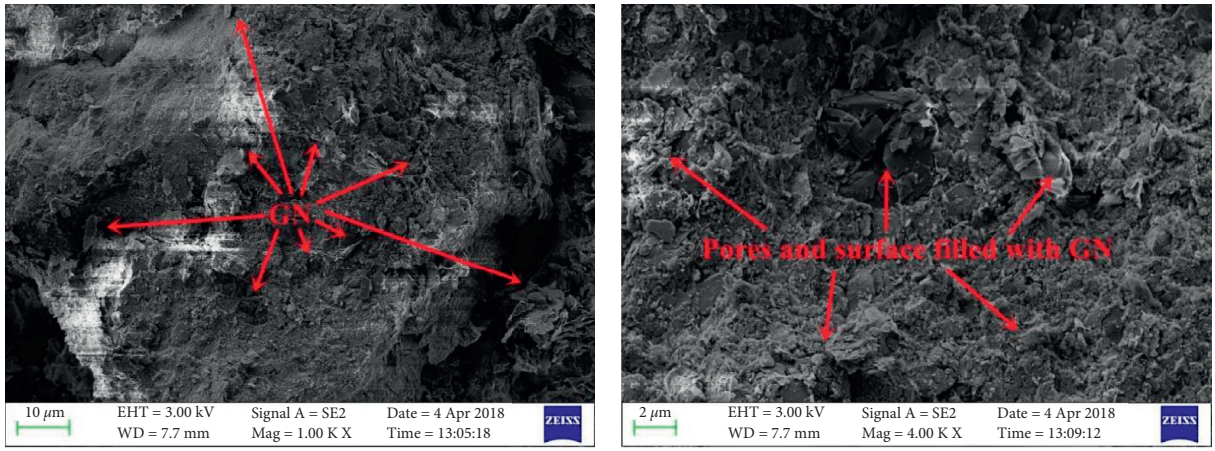

(e) (f)

Figure 17: SEM of laterite and GN-laterite, (a) $\rho_d = 1.40\ g/cm^3$, $M = 0\%$, 1 000×, (b) $\rho_d = 1.40\ g/cm^3$, $M = 0\%$, 4 000×, (c) $\rho_d = 1.50\ g/cm^3$, $M = 0\%$, 1 000×, (d) $\rho_d = 1.50\ g/cm^3$, $M = 0\%$, 4 000×, (e) $\rho_d = 1.40\ g/cm^3$, $M = 1.0\%$, 1 000×, and (f) $\rho_d = 1.40\ g/cm^3$, $M = 1.0\%$, 4 000×.

After adding GN, the particle surfaces of the laterite become layered, changing from agglomerated structure to flocculent structure. The basic unit or structural unit of laterite is basically inlaid contact mode. The rough area of the surfaces of the soil particle is improved, and the surfaces are uneven. The degree is reduced, and the texture of GN-laterite is uniform and has a certain directionality. The main reason is that GN enhances the overall cementation of the particles and changes the structure of the laterite from porous to dense structure. After being magnified by 4 000 times, the laterite particles and the surrounding pores are filled with GN. GN has a certain wrapping effect on fine particles with different shapes, which makes the points-surfaces contact between the soil particles change to the surfaces-surfaces contact. At the same time, it connects the originally relatively independent adjacent particle clusters together, the bonding strength is large, the interparticle interlocking connection is closer, making the structure of the skeleton structure stable, the large pores between the skeletons are significantly smaller, and the structural stability is stronger.

On the other hand, GN has smaller particle size, larger specific surface area, and higher surface energy, so they have nano effects such as small size effect, quantum size effect, and surface effect, and GN themselves have strong adsorption, structural stability, high temperature resistance, and other properties. Originally, many clay minerals aggregate together, forming an unstable overhead structure. The cohesive force between the particles mainly comes from the cementation of cement, but this cementing force is relatively weak. The overhead structure will be destroyed under certain engineering force. When GN is mixed into laterite, they are adsorbed on the surface of the laterite particles or filled in the pores. Due to nanoeffects, GN has a great specific surface energy and strong adsorption, and they are involved in the cementation between particles together. The cementation force increases the mutual attraction between the laterite particles, the soil particles gather, and the contact points between the laterite particles increase. The electrostatic attraction and van der Waals force between soil particles are enhanced, resulting in the increase of the cohesion and shear strength of the laterite and the decrease of the compressibility and permeability coefficient. The mechanical properties of laterite are determined by factors such as the state of cohesion between soil particles, friction properties, and the properties of bound water. When GN is mixed with laterite, their cation exchange capacity is enhanced, and the ion-electrostatic force increases, so that the water film of the diffusion layer in the electric double layer becomes thinner, the distance between the particles is relatively reduced, the contact area increases, and the soil structure gradually stabilizes. While the GN content is too large, the lubrication is increased due to the increase of GN content, and a continuous film layer will be formed in the laterite. This GN film layer is equivalent to a structural weak surface, which will be preferentially damaged under the action of external force. As a result, the shear strength, compressibility, and permeability coefficient of laterite cannot increase significantly or even decreased.

5. Conclusions

In this paper, graphite nanoparticles (GN) were selected as the admixture of laterite to further study the influence of GN on the material composition, mechanical properties, and microstructure of laterite, as well as the micromechanism that causes changes in macromechanical properties of laterite. The following conclusions are drawn:

(1) The increase of dry density is correlated with the improvement of shear strength and compression performance of Guilin laterite, that is, the higher the dry density is, the more compact the soil is. The results show that the fine soil particles and GN will be more dispersed, fill into the pores between the soil particles, enhance the occlusion, make the soil structure tend to be complete, the shear strength and

compression performance of laterite will be enhanced, but the growth rate will decline when the dry density is greater than 1.40 g/cm^3.

(2) With the addition of GN in laterite, the shear strength, compressive strength, and impermeability of laterite have been improved. When the content of GN is 0%–1.0%, the shear strength, compression performance, and impermeability performance will increase with the increase of the content. While the content of GN is 1.0%–2.0%, the shear strength decreases with the increase of the content, and the increase of compressive strength and impermeable strength decreases, but they are still more stable than that of plain laterite. The optimal content is about 1.0%, that is, a proper amount of GN is the most effective for improving the shear strength of laterite. Under different confining pressures, the trend of shear strength changing with dry density is similar.

(3) GN reduces the water film thickness of the laterite particle diffusion layer by changing the mineral composition and chemical composition of the laterite, so that the surfaces of the laterite particles are layered and the degree of unevenness is reduced, thereby enhancing the interparticle bonding force, electrostatic force, and other forces. GN has a certain enveloping effect on the soil particles, which increases the contact areas of structural units and reduces the pores between particles. It connects relatively independent adjacent particles together, and the structural framework is gradually stabilized.

Data Availability

The authors declare that all the data were presented in the figures and tables in the manuscript. The data used to support the findings of this study are available from the corresponding author upon request.

Conflicts of Interest

The authors declare that they have no conflicts of interest.

Authors' Contributions

Yuhao Gao wrote the original draft, conceptualized the study, and acquired funding. Jianzhong Li reviewed and edited the manuscript, supervised the study, and acquired funding. Yuxin Zhang investigated the study and contributed to data curation. Xu Sun investigated and validated the study. Leiyong Yang investigated the study and provided resources.

Acknowledgments

The authors are grateful for the support provided by the National Natural Science Foundation of China (Grant no. 41572269), Hunan Provincial Innovation Foundation for Postgraduate (Grant no. CX20200303), and the Fundamental Research Funds for the Central Universities of Central South University (Grant no. 2020zzts658).

References

[1] N. O. Attoh-Okine, "Application of genetic-based neural network to lateritic soil strength modeling," *Construction and Building Materials*, vol. 18, no. 8, pp. 619–623, 2004.

[2] G. Gao, "The distribution and geotechnical properties of loess soils, lateritic soils and clayey soils in China," *Engineering Geology*, vol. 42, no. 1, pp. 95–104, 1996.

[3] L. D. Jerez, O. E. Gómez, and C. A. Murillo, "Stabilization of Colombian lateritic soil with a hydrophobic compound (organosilane)," *International Journal of Pavement Research and Technology*, vol. 11, no. 6, pp. 639–646, 2018.

[4] P. Sarma, S. Singh, and M. Kaur, "Optimization of sisal fibre and rice husk ash usage on lateritic soil for construction of roadway," *Materials Today: Proceedings*, vol. 33, pp. 1720–1726, 2020.

[5] Z. Lin, "On the engineering classification of laterite," *Chinese Journal of Geotechnical Engineering*, vol. 11, no. 1, pp. 85–96, 1989, in Chinese.

[6] Y. Zhao, L. Kong, A. Guo, and Y. Tuo, "Mechanical behaviors and water-sensitive properties of intact Guangxi laterite," *Rock and Soil Mechanics*, vol. 24, no. 4, pp. 568–572, 2003, in Chinese.

[7] Y. Chen, H. Lei, Y. He, and W. Ye, "Experimental study of permeability of bentonite-laterite mixtures for salt solutions," *Journal of Central South University*, vol. 49, no. 4, pp. 146–151, 2018, in Chinese.

[8] B. Fu, L. Huang, and L. Fang, "Analysis of geohazard origin in the laterite area," *Chinese Journal of Geological Hazard and Control*, vol. 9, no. 4, pp. 13–18, 1998, in Chinese.

[9] S. Li, Z. Liu, and J. Meng, "Effect of pH value on boundary water content of red clay in Guilin and its mechanism," *Chinese Journal of Geotechnical Engineering*, vol. 39, no. 10, pp. 1814–1822, 2017, in Chinese.

[10] G. Cai, A. Zhou, Y. Liu, R. Xu, and C. Zhao, "Soil water retention behavior and microstructure evolution of lateritic soil in the suction range of 0-286.7 MPa," *Acta Geotechnica*, vol. 15, no. 12, pp. 3327–3341, 2020.

[11] C. R. Kaze, G. L. Lecomte-Nana, E. Kamseu et al., "Mechanical and physical properties of inorganic polymer cement made of iron-rich laterite and lateritic clay: a comparative study," *Cement and Concrete Research*, vol. 140, Article ID 106320, 2021.

[12] R. N. Rosli, M. R. Selamat, and M. H. Ramli, "Shear strength and permeability properties of lateritic soils from North West Malaysia due to extended compaction," *Materials Today: Proceedings*, vol. 17, pp. 630–639, 2019.

[13] D. Sun, G. You, Z. Annan, and S. Daichao, "Soil-water retention curves and microstructures of undisturbed and compacted Guilin lateritic clay," *Bulletin of Engineering Geology and the Environment*, vol. 75, no. 2, pp. 781–791, 2016.

[14] Y. He, R. Huang, Y. Cheng, and W. Ye, "Water retention properties of deformable compacted red clay induced by wetting and drying," *Journal of Central South University*, vol. 47, no. 1, pp. 143–148, 2016, in Chinese.

[15] J. O. Afolayan and C. M. O. Nwaiwu, "Reliability-based assessment of compacted lateritic soil liners," *Computers and Geotechnics*, vol. 32, no. 7, pp. 505–519, 2005.

[16] J. Chen, F. Dai, L. Xu et al., "Properties and microstructure of a natural slip zone in loose deposits of red beds, southwestern China," *Engineering Geology*, vol. 183, pp. 53–64, 2014.

[17] Y. Xu, Z. Zeng, D. a. Sun, and H. Lv, "Comparative study on thermal properties of undisturbed and compacted lateritic soils subjected to drying and wetting," *Engineering Geology*, vol. 277, Article ID 105800, 2020.

[18] Z. Wan, A. Guo, Y. Tan, L. B. chen, and W. Y. Zhong, "Study of embankment filled technology of laterite soil in Southwest Hunan," *Rock and Soil Mechanics*, vol. 32, no. 8, pp. 2281–2286, 2011, in Chinese.

[19] Q. Nie, Y. Wang, S. Liang, and Q. X. Zhang, "Water-sensitivity of compacted laterite clays in jingxi of Guangxi region," *Rock and Soil Mechanics*, vol. 31, no. 4, pp. 1134–1138, 2010, in Chinese.

[20] Y. Tan, L. Kong, A. Guo, and X. Feng, "Discussion on the compaction degree index of subgrade filled with laterite," *Rock and Soil Mechanics*, vol. 31, no. 3, pp. 851–855, 2010, in Chinese.

[21] C. Chen, S. Zhu, G. Zhang, F. Mao, and H. Cai, "Time-dependent load transfer behavior of grouted anchors in laterite," *Computers and Geotechnics*, vol. 132, no. 4, Article ID 103969, 2021.

[22] M. F. d. Silva, M. M. P. Ribeiro, A. P. Furlan, T. Glauco, and P. Fabbri, "Effect of compaction water content and stress ratio on permanent deformation of a subgrade lateritic soil," *Transportation Geotechnics*, vol. 26, Article ID 100443, 2021.

[23] A. Cheshomi, A. Eshaghi, and J. Hassanpour, "Effect of lime and fly ash on swelling percentage and Atterberg limits of sulfate-bearing clay," *Applied Clay Science*, vol. 135, pp. 190–198, 2017.

[24] R. K. Goswami and C. Mahanta, "Leaching characteristics of residual lateritic soils stabilised with fly ash and lime for geotechnical applications," *Waste Management*, vol. 27, no. 4, pp. 466–481, 2007.

[25] S. K. Pal and A. Ghosh, "Hydraulic conductivity of fly ash-montmorillonite clay mixtures," *Indian Geotechnical Journal*, vol. 43, no. 1, pp. 47–61, 2013.

[26] K. V. Bicalho, Y. Boussafir, and Y.-J. Cui, "Performance of an instrumented embankment constructed with lime-treated silty clay during four-years in the Northeast of France," *Transportation Geotechnics*, vol. 17, pp. 100–116, 2018.

[27] I. I. Obianyo, A. P. Onwualu, and A. B. O. Soboyejo, "Mechanical behaviour of lateritic soil stabilized with bone ash and hydrated lime for sustainable building applications," *Case Studies in Construction Materials*, vol. 12, Article ID e00331, 2020.

[28] R. Ignat, S. Baker, M. Holmén, and S. Larsson, "Triaxial extension and tension tests on lime-cement-improved clay," *Soils and Foundations*, vol. 59, no. 5, pp. 1399–1416, 2019.

[29] O. E. Oluwatuyi, B. O. Adeola, E. A. Alhassan et al., "Ameliorating effect of milled eggshell on cement stabilized lateritic soil for highway construction," *Case Studies in Construction Materials*, vol. 9, Article ID e00191, 2018.

[30] S. D. Khadka, P. W. Jayawickrama, S. Senadheera, and B. Segvic, "Stabilization of highly expansive soils containing sulfate using metakaolin and fly ash based geopolymer modified with lime and gypsum," *Transportation Geotechnics*, vol. 23, Article ID 100327, 2020.

[31] M. R. Abdi, A. Ghalandarzadeh, and L. S. Chafi, "An investigation into the effects of lime on compressive and shear strength characteristics of fiber-reinforced clays," *Journal of Rock Mechanics and Geotechnical Engineering*, vol. 13, no. 4, 2021.

[32] O. E. Oluwatuyi, O. O. Ojuri, and A. Khoshghalb, "Cement-lime stabilization of crude oil contaminated kaolin clay," *Journal of Rock Mechanics and Geotechnical Engineering*, vol. 12, no. 1, pp. 160–167, 2020.

[33] Q. Cheng, K. Yao, and Y. Liu, "Stress-dependent behavior of marine clay admixed with fly-ash-blended cement," *International Journal of Pavement Research and Technology*, vol. 11, no. 6, pp. 611–616, 2018.

[34] P. Wang, Y. Hu, and H. Cheng, "Municipal solid waste (MSW) incineration fly ash as an important source of heavy metal pollution in China," *Environmental Pollution*, vol. 252, pp. 461–475, 2019.

[35] I. Khan and R. Umar, "Environmental risk assessment of coal fly ash on soil and groundwater quality, Aligarh, India," *Groundwater for Sustainable Development*, vol. 8, pp. 346–357, 2019.

[36] D. Gupta, U. Rai, R. Tripathi, and M. Inouhe, "Impacts of fly-ash on soil and plant responses," *Journal of Plant Research*, vol. 115, no. 6, pp. 401–409, 2002.

[37] Y. Tan, S. Zhan, K. Shen, Z. Q. Jun, and M. H. Jun, "Effect of hardening and intergranular cementation on the surface of treated aggregate laterite," *Rock and Soil Mechanics*, vol. 42, no. 2, pp. 361–368, 2021, in Chinese.

[38] Y. Tan, M. Hu, and D. Li, "Effects of agglomerate size on California bearing ratio of lime treated lateritic soils," *International Journal of Sustainable Built Environment*, vol. 5, no. 1, pp. 168–175, 2016.

[39] K. A. Olatunde, P. A. Sosanya, B. S. Bada, Z. O. Ojekunlea, and S. A. Abdussalaam, "Distribution and ecological risk assessment of heavy metals in soils around a major cement factory, Ibese, Nigeria," *Scientific African*, vol. 9, Article ID e00496, 2020.

[40] E. Adeyanju and C. A. Okeke, "Exposure effect to cement dust pollution: a mini review," *SN Applied Sciences*, vol. 1, no. 12, pp. 1–17, 2019.

[41] L. Cutillas-Barreiro, P. Pérez-Rodríguez, A. Gómez-Armesto et al., "Lithological and land-use based assessment of heavy metal pollution in soils surrounding a cement plant in SW Europe," *The Science of the Total Environment*, vol. 562, pp. 179–190, 2016.

[42] S. N. Singh and D. N. Rao, "Growth of wheat plants exposed to cement dust pollution," *Water, Air, and Soil Pollution*, vol. 14, no. 1, pp. 241–249, 1980.

[43] H.-L. Luo, D.-H. Hsiao, D.-F. Lin, and C.-K. Lin, "Cohesive soil stabilized using sewage sludge ash/cement and nano aluminum oxide," *International Journal of Transportation Science and Technology*, vol. 1, no. 1, pp. 83–99, 2012.

[44] K. Yao, W. Wang, N. Li, C. Zhang, and L. Wang, "Investigation on strength and microstructure characteristics of nano-MgO admixed with cemented soft soil," *Construction and Building Materials*, vol. 206, pp. 160–168, 2019.

[45] A. Kalhor, M. Ghazavi, M. Roustaei, and S. M. Mirhosseini, "Influence of nano-SiO2 on geotechnical properties of fine soils subjected to freeze-thaw cycles," *Cold Regions Science and Technology*, vol. 161, pp. 129–136, 2019.

[46] T. Meng, Y. Qiang, A. Hu, C. Xu, and L. Lin, "Effect of compound nano-CaCO3 addition on strength development and microstructure of cement-stabilized soil in the marine environment," *Construction and Building Materials*, vol. 151, pp. 775–781, 2017.

[47] V. P. Nguyen, K. T. T. Nguyen, L. T. Ton et al., "Dual-electronic nanomaterial (synthetic clay) for effective removal of toxic cationic and oxyanionic metal ions from water," *Journal of Nanomaterials*, vol. 2020, Article ID 1783749, 11 pages, 2020.

[48] N. Hamed, M. S. El-Feky, M. Kohail, and E.-S. A. R. Nasr, "Effect of nano-clay de-agglomeration on mechanical

properties of concrete," *Construction and Building Materials*, vol. 205, pp. 245–256, 2019.

[49] M. Khodaparast, A. M. Rajabi, and M. Mohammadi, "Mechanical properties of silty clay soil treated with a mixture of lime and zinc oxide nanoparticles," *Construction and Building Materials*, vol. 281, Article ID 122548, 2021.

[50] A. J. Choobbasti, M. A. Samakoosh, and S. S. Kutanaei, "Mechanical properties soil stabilized with nano calcium carbonate and reinforced with carpet waste fibers," *Construction and Building Materials*, vol. 211, pp. 1094–1104, 2019.

[51] M. Monsif, A. Zerouale, N. I. Kandri et al., "Multifunctional epoxy/nanocomposites based on natural Moroccan clays with high antimicrobial activity: morphological, thermal and mechanical properties," *Journal of Nanomaterials*, vol. 2019, Article ID 2810901, 12 pages, 2019.

[52] A. Divya, S. Shrihari, and H. Ramesh, "Predictive simulation of leachate transport in a coastal lateritic aquifer when remediated with reactive barrier of nano iron," *Groundwater for Sustainable Development*, vol. 11, Article ID 100382, 2020.

[53] Q. Li, L. Chen, H. Ma, and C. H. Huang, "Enhanced heat transfer characteristics of graphite concrete and its application in energy piles," *Advances in Materials Science and Engineering*, vol. 2018, Article ID 8142392, 12 pages, 2018.

[54] H. Liu, K. Liu, Z. Lan, and D. Zhang, "Mechanical and electrical characteristics of graphite tailing concrete," *Advances in Materials Science and Engineering*, vol. 2018, Article ID 9297628, 9 pages, 2018.

[55] A. Karaipekli, A. Sarı, and K. Kaygusuz, "Thermal conductivity improvement of stearic acid using expanded graphite and carbon fiber for energy storage applications," *Renewable Energy*, vol. 32, no. 13, pp. 2201–2210, 2007.

[56] M. Jobmann and G. Buntebarth, "Influence of graphite and quartz addition on the thermo–physical properties of bentonite for sealing heat-generating radioactive waste," *Applied Clay Science*, vol. 44, no. 3-4, pp. 206–210, 2009.

[57] X. Liu, S. S. C. Congress, G. Cai, and S. Liu, "Performance evaluation of soil mixtures treated with graphite and used as barrier fill material for high-level radioactive waste repository," *Acta Geotechnica*, vol. 16, no. 5, pp. 1487–1507, 2021.

[58] X. Liu, G. Cai, L. Liu, S. Liu, and A. J. Puppala, "Thermo-hydro-mechanical properties of bentonite-sand-graphite-polypropylene fiber mixtures as buffer materials for a high-level radioactive waste repository," *International Journal of Heat and Mass Transfer*, vol. 141, pp. 981–994, 2019.

[59] D. Priyankar, Z. Ali, M. Nagaral, P. Rathna kumar, V. Muthuraman, and M. D. Umar, "Microstructure and evolution of mechanical properties of Cu-Sn alloy with graphite and nano zirconium oxide particulates," *Materials Today: Proceedings*, vol. 54, 2021.

[60] X. Cui, S. Sun, B. Han et al., "Mechanical, thermal and electromagnetic properties of nanographite platelets modified cementitious composites," *Composites Part A: Applied Science and Manufacturing*, vol. 93, pp. 49–58, 2017.

[61] V.-H. Nguyen, S. A. Delbari, A. Sabahi Namini et al., "Microstructural, mechanical and friction properties of nano-graphite and h-BN added TiC-based composites," *Ceramics International*, vol. 46, no. 18, pp. 28969–28979, 2020.

[62] Y. Li, H. Zhang, Z. Huang, E. Biloti, and T. Peijis, "Graphite nanoplatelet modified epoxy resin for carbon fibre reinforced plastics with enhanced properties," *Journal of Nanomaterials*, vol. 2017, Article ID 5194872, 10 pages, 2017.

[63] J.-Z. Liang, Q. Du, G. C.-P. Tsui, and C.-Y. Tang, "Tensile properties of graphene nano-platelets reinforced polypropylene composites," *Composites Part B: Engineering*, vol. 95, pp. 166–171, 2016.

[64] W. Meng and K. H. Khayat, "Mechanical properties of ultra-high-performance concrete enhanced with graphite nanoplatelets and carbon nanofibers," *Composites Part B: Engineering*, vol. 107, pp. 113–122, 2016.

[65] M. K. Gupta and J. Bijwe, "A complex interdependence of dispersant in nano-suspensions with varying amount of graphite particles on its stability and tribological performance," *Tribology International*, vol. 142, 2020.

[66] B. N. Yuyuths Gowda, M. R. Haseebuddin, B. Pal, and R. Keshavamurthy, "Mechanical and wear behaviour of graphite nano filler reinforced Al 6061 composites," *Materials Today: Proceedings*, vol. 46, pp. 4504–4509, 2021.